Technical Note: Characterization of custom 3D printed multimodality imaging phantoms

Matthew F. Bieniosek
Department of Electrical Engineering, Stanford University, 350 Serra Mall, Stanford, California 94305

Brian J. Lee
Department of Mechanical Engineering, Stanford University, 440 Escondido Mall, Stanford, California 94305

Craig S. Levin[a)]
Departments of Radiology, Physics, Bioengineering and Electrical Engineering, Stanford University, 300 Pasteur Dr., Stanford, California 94305-5128

(Received 10 December 2014; revised 2 August 2015; accepted for publication 29 August 2015; published 17 September 2015)

Purpose: Imaging phantoms are important tools for researchers and technicians, but they can be costly and difficult to customize. Three dimensional (3D) printing is a widely available rapid prototyping technique that enables the fabrication of objects with 3D computer generated geometries. It is ideal for quickly producing customized, low cost, multimodal, reusable imaging phantoms. This work validates the use of 3D printed phantoms by comparing CT and PET scans of a 3D printed phantom and a commercial "Micro Deluxe" phantom. This report also presents results from a customized 3D printed PET/MRI phantom, and a customized high resolution imaging phantom with sub-mm features.

Methods: CT and PET scans of a 3D printed phantom and a commercial Micro Deluxe (Data Spectrum Corporation, USA) phantom with 1.2, 1.6, 2.4, 3.2, 4.0, and 4.8 mm diameter hot rods were acquired. The measured PET and CT rod sizes, activities, and attenuation coefficients were compared. A PET/MRI scan of a custom 3D printed phantom with hot and cold rods was performed, with photon attenuation and normalization measurements performed with a separate 3D printed normalization phantom. X-ray transmission scans of a customized two level high resolution 3D printed phantom with sub-mm features were also performed.

Results: Results show very good agreement between commercial and 3D printed micro deluxe phantoms with less than 3% difference in CT measured rod diameter, less than 5% difference in PET measured rod diameter, and a maximum of 6.2% difference in average rod activity from a 10 min, 333 kBq/ml (9 μCi/ml) Siemens Inveon (Siemens Healthcare, Germany) PET scan. In all cases, these differences were within the measurement uncertainties of our setups. PET/MRI scans successfully identified 3D printed hot and cold rods on PET and MRI modalities. X-ray projection images of a 3D printed high resolution phantom identified features as small as 350 μm wide.

Conclusions: This work shows that 3D printed phantoms can be functionally equivalent to commercially available phantoms. They are a viable option for quickly distributing and fabricating low cost, customized phantoms. [http://dx.doi.org/10.1118/1.4930803]

Key words: 3D printing, rapid prototyping, phantoms, PET, MRI

1. INTRODUCTION

Imaging phantoms are used as a well known ground truth to test hardware performance, reconstruction techniques, segmentation algorithms, motion correction, and any other imaging performance metrics without exposing patients or animals to unnecessary testing. Phantoms can take a number of different shapes depending on the parameters to be tested. Several types of imaging phantoms exist, including plastic or glass cavities, suspensions of gel[1] or wax,[2] and ink-jet printed 2D surfaces.[3] Commercially available phantoms can be expensive and difficult to customize, while making a phantom with a precise customized geometry may be very difficult and time consuming. Three dimensional (3D) printers offer an attractive alternative to traditional phantom construction techniques. 3D printers automatically build objects defined by a computer model. In the past, they have been used to create both single-use[4] and refillable phantoms.[5,6] As 3D printing technology improves, the technique is also becoming increasingly accurate, versatile, and accessible. Low cost 3D printers can be purchased for as little as a few hundred dollars. In this work, we seek to compare the performance of a 3D printed phantom to a traditional commercial phantom to validate its use in testing of experimental PET/CT and PET/MRI instrumentation and show highly customized phantom geometries that are practical to produce using 3D printing.

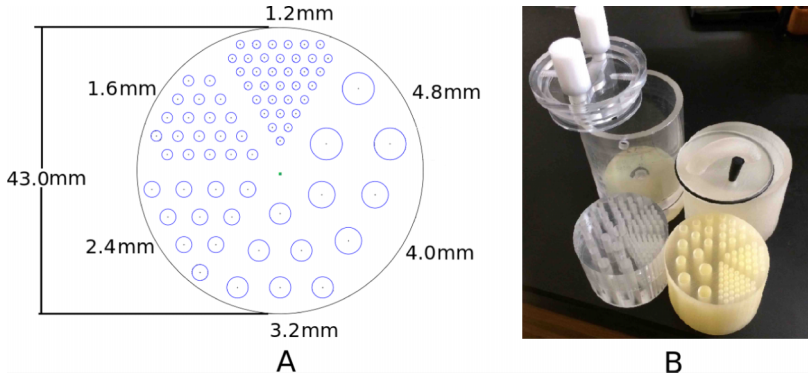

FIG. 1. (A) Diagram and (B) photograph of the 3D printed and commercial micro deluxe phantoms. The 3D printed micro deluxe phantom is on the right of the photograph, and the commercial micro deluxe phantom is on the left.

2. MATERIALS AND METHODS

2.A. PET/CT

To validate our phantom fabrication process, a commercial "Micro Deluxe" phantom (Data Spectrum Corporation, USA) (referred to henceforth as "commercial micro deluxe") and a comparable 3D printed phantom (referred to henceforth as "3D printed micro deluxe") were scanned using high resolution CT and PET modalities. Each phantom has hollow wells to be filled with imaging agents. The dimensions of these wells were designed to be the same for the commercial and 3D printed micro deluxe phantoms (see Fig. 1). The 3D printed micro deluxe phantom can be closed with a cap that was also fabricated by the 3D printer, along with an O-ring and stopper for a tight seal.

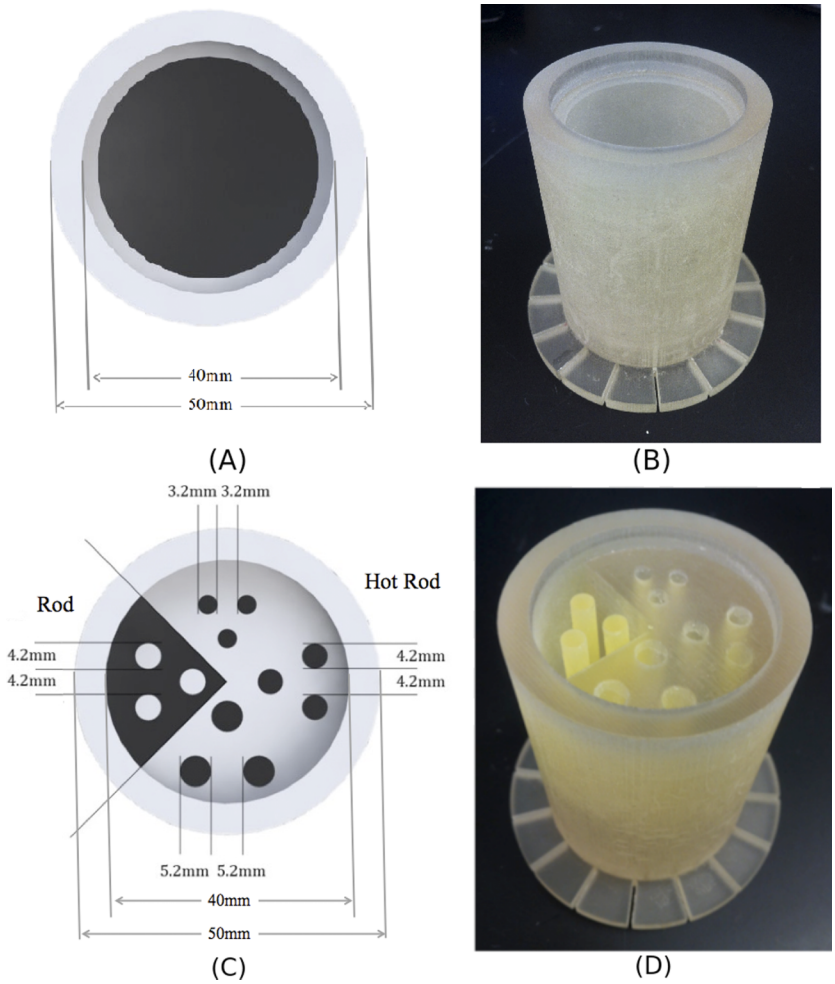

FIG. 2. (A) Diagram and (B) photograph of 3D printed PET/MRI normalization phantom. (C) Diagram and (D) photograph of a 3D printed PET/MRI resolution phantom with hot and cold rods.

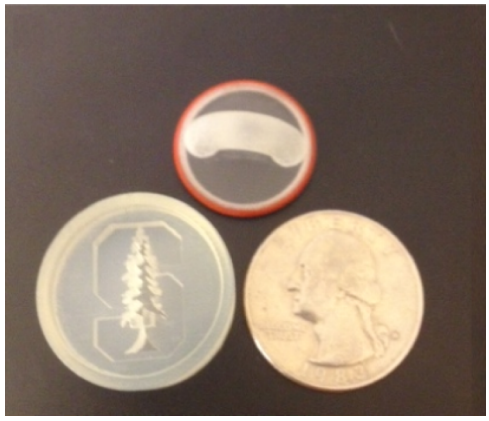

FIG. 3. A 3D printed two-level high resolution phantom showing the Stanford University logo with visible branches from 1 mm to 350 μm wide.

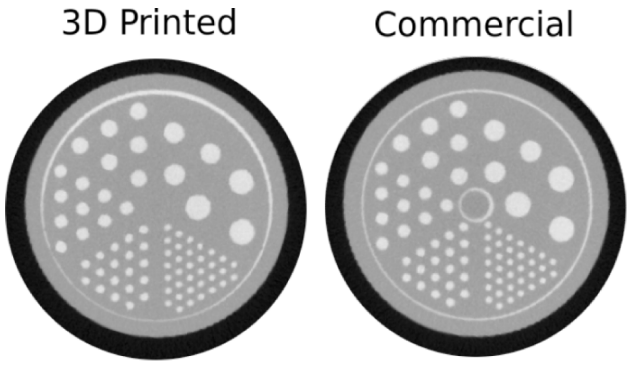

FIG. 4. CT cross sections of each micro deluxe phantom filled with iodine contrast agent.

The 3D printed micro deluxe phantom was fabricated with a ProJet HD3500 (3D Systems, USA), which prints plastics with a resolution of $750\times750\times890$ (x–y–z) dots/in. and an accuracy of less than 0.002 in. (51 μm)/in. of part dimension. The plastic used in our 3D printer was VisiJet M3 Crystal with a density of 1.02 g/cm^3 (for other material properties, see Ref. 7). The commercial micro deluxe phantom is acrylic. CT images of the phantoms filled with iodine contrast agent were taken using a rotating stage and a Varian PaxScan 4030CB flat panel x-ray detector (Varian Medical Systems, Inc, USA), which has a pixel pitch of 194 μm. 10 min PET scans of the phantoms filled with 333 kBq/ml (9 μCi/ml) F-18 were taken while centered in a Siemens Inveon PET scanner (Siemens Healthcare, Germany). Hot areas were defined as voxels with activity in the highest 0.4 ‰.

2.B. PET/MRI

A resolution phantom with both hot and cold rods [see Figs. 2(C) and 2(D)] was 3D printed for the study of image quality in an experimental PET/MRI insert.[8] Images of this phantom with 200 μCi of FDG solution were taken in a GE Discovery MR750w 3 T MRI (GE Healthcare, USA) with the PET insert. Images were reconstructed with a 3D list-mode MLEM algorithm.[9] Photon attenuation and normalization corrections were performed using a 3D printed normalization phantom, which is a cylindrical phantom of the same outer dimension and attenuation properties as the resolution phantom we are imaging [see Figs. 2(A) and 2(B)]. A correction was applied to the normalization map to compensate for the attenuation and the overestimate of sensitivity toward the scanner trans-axial center that results from a cylindrical geometry of activity.

2.C. High resolution phantom

A two level phantom for an ultra-high resolution PET scanner was also produced (see Fig. 3). The phantom shows customized shapes and extremely high resolution (small branches are 350 μm thick) features that can be created with the 3D printer. The phantom was scanned while empty and while filled with iodine contrast agent using a Varian PaxScan 4030CB flat panel x-ray detector.

3. RESULTS

3.A. PET/CT

The 3D printed micro deluxe phantom showed no significant differences from the commercial micro deluxe phantom (see Table I). The CT scan (seen in Fig. 4) shows average rod diameters that differ a maximum of 2.36% between the two phantoms. This difference was within the measurement uncertainty of the setup, which was determined by taking the standard deviation of the measurements for the different

TABLE I. Summary of results with one standard deviation measurement uncertainty.

	Nominal rod diameter					
	1.2 mm	1.6 mm	2.4 mm	3.2 mm	4.0 mm	4.8 mm
CT diameter 3D printed micro deluxe (mm)	1.23 ± 0.04	1.62 ± 0.05	2.46 ± 0.10	3.20 ± 0.07	3.91 ± 0.05	4.74 ± 0.07
CT diameter commercial micro deluxe (mm)	1.23 ± 0.04	1.66 ± 0.03	2.40 ± 0.02	3.21 ± 0.02	3.96 ± 0.01	4.78 ± 0.01
Percent difference	0.07	−2.36	2.30	−0.26	−1.20	−1.09
PET diameter 3D printed micro deluxe (mm)	N/A	1.69 ± 0.25	2.76 ± 0.23	3.67 ± 0.21	4.31 ± 0.13	5.21 ± 0.12
PET diameter commercial micro deluxe (mm)	N/A	1.75 ± 0.23	2.64 ± 0.21	3.70 ± 0.16	4.28 ± 0.08	5.17 ± 0.04
Percent difference	N/A	−3.22	4.63	−0.90	0.67	0.91
Normalized activity, 3D printed micro deluxe	N/A	0.54 ± 0.05	0.74 ± 0.06	0.83 ± 0.04	0.94 ± 0.04	0.98 ± 0.03
Normalized activity, commercial micro deluxe	N/A	0.55 ± 0.04	0.70 ± 0.05	0.80 ± 0.05	0.92 ± 0.02	1.00 ± 0.02
Percent difference	N/A	−2.16	6.18	3.45	1.53	−2.01

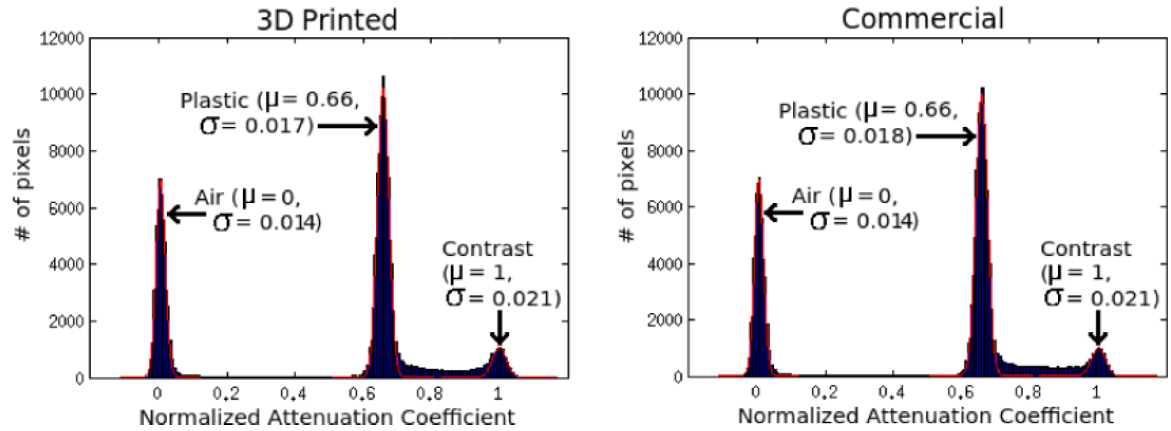

FIG. 5. Normalized pixel intensity of each micro deluxe CT scan. Clear peaks are seen for pixels in areas of air, plastic, liquid contrast agent. The region corresponding to plastic in the 3D printed micro deluxe phantom has the same attenuation coefficient as the same region in the commercial micro deluxe phantom.

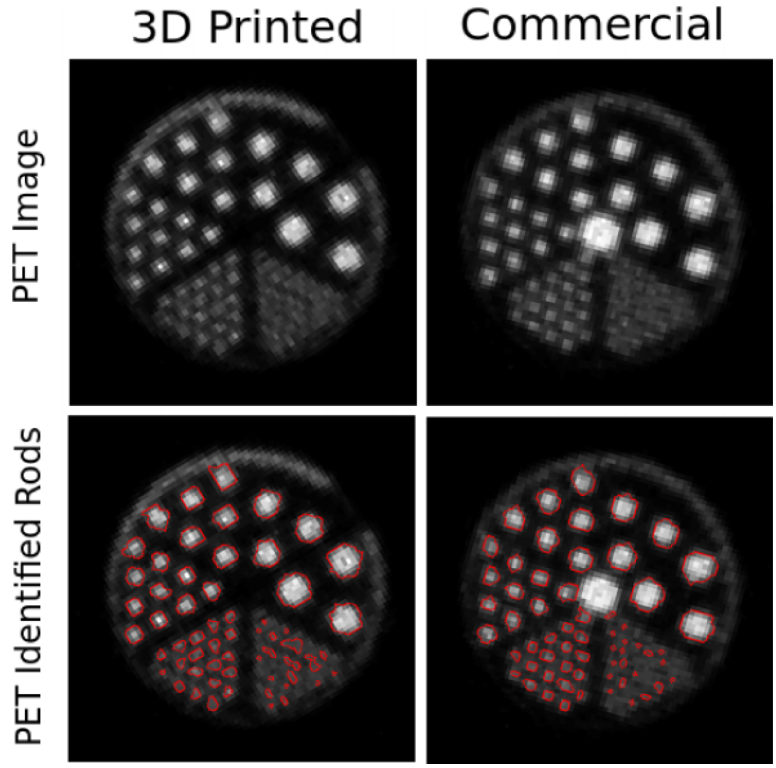

FIG. 6. PET cross sections of each micro deluxe phantom filled with a solution containing 333 kBq/ml (9 μCi/ml) F-18 with and without the identified hot areas above an activity threshold outlined.

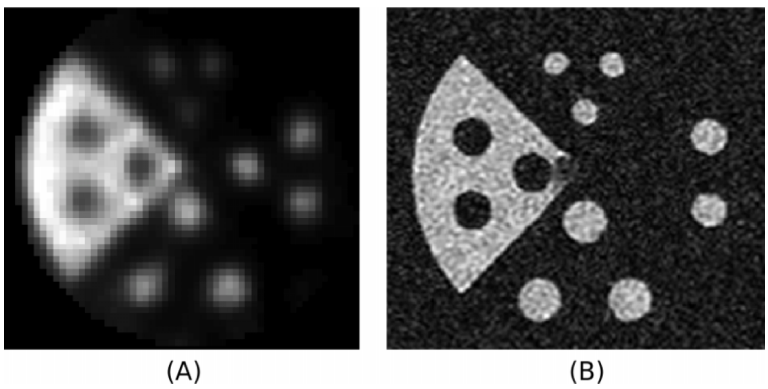

FIG. 7. (A) Normalized PET and (B) MRI images of a 3D printed PET/MRI resolution phantom with hot and cold rods.

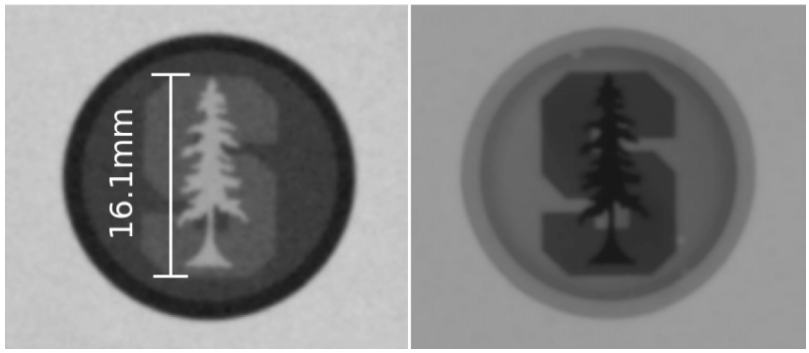

FIG. 8. X-ray projection images are shown with the high resolution phantom filled with air (left) and iodine contrast agent (right).

rods of each size. The attenuation coefficients of the phantom materials were also quite similar. When normalized to the attenuation of the contrast agent, both phantoms show a mean of 0.66 (see Fig. 5).

The PET scan also showed good agreement between phantoms (see Fig. 6). In both phantoms, rods larger than 1.2 mm were identified. The average identified rod diameters differ by a maximum of 4.63%. The average mean activity in the rods differed by no more than 6.18%. Again, these differences were within the measurement uncertainty of our setup.

3.B. PET/MRI

Images were also produced of the 3D printed PET/MRI resolution phantom with hot and cold rods for the experimental PET/MRI system after photon attenuation and normalization corrections (see Fig. 7). The PET/MRI images show hot and cold rods visible on both PET and MRI modalities.

3.C. High resolution phantom

Images of the two-level high resolution phantom showing the Stanford University logo are seen in Fig. 8. Features as small as 350 μm are visible on the x-ray projection images.

4. DISCUSSION

This work describes a 3D printed micro deluxe phantom with no statistically significant differences from a commercial micro deluxe phantom. The measured rod diameters agree within measurement uncertainty (see Table I). The plastic materials of the two phantoms also have very similar imaging properties (see Fig. 5).

3D printing also allows for the fabrication of highly customized multimodal phantoms as seen in Figs. 2 and 3. These phantoms could be used to test imaging properties in ways standard phantoms could not. Once designed, these phantoms can be freely shared between researches via online repositories or supplemental files in online journals. The phantoms described in this paper can be viewed at stanford.edu/~mbieni/Phantoms/.

3D printers are capable of producing a wide variety of phantoms. The 3D printer used for this work had a feature precision of 0.002 in. (51 μm). Actual structures built are mostly limited by the mechanical strength of the 3D printed material. Phantom wall thicknesses below 0.5 mm on many 3D printers are not recommended due to mechanical constraints, but these constraints are highly dependent on printing material and phantom structure.

The high resolution of 3D printing with feature sizes down to 350 μm shown in this paper also suggests that phantoms specifically for CT and MRI quality control may also be fabricated using this technique. While the plastic used in the work was not visible in our MRI data, the 3D printing industry has been growing intensely and various manufacturing material types are available. In the future, a 3D printable material visible to MRI maybe available.

5. CONCLUSIONS

In this work, we have fabricated and scanned a 3D printed phantom replicating a commercial micro deluxe PET phantom. The phantoms appear very similar under both PET and CT scans. The difference in measured rod diameters was less than the measurement uncertainty. PET images also show activity levels within measurement uncertainties. Studies of PET/MRI and high resolution phantoms were also presented. This work validates the use of 3D printed phantoms, which can be used to make highly customized, cost effective, multimodal phantoms. It also enables the easy sharing of digital phantom designs that can be produced by 3D printers at different locations.

ACKNOWLEDGMENTS

The authors thank Frezghi Habte and Alex Grant for their help with the PET imaging as well as David Hsu and Waldo Hinshaw for their help with the x-ray imaging. This work was supported in part by NIH research Grant No. R01 EB011552 and NIH training Grant No. 1F31CA171573-01.

[a]Author to whom correspondence should be addressed. Electronic mail: cslevin@stanford.edu

[1]J. S. Huber, Q. Peng, and W. Moses, "Multi-modality phantom development," IEEE Trans. Nucl. Sci. **56**(5), 2722–2727 (2009).

[2]T. G. Turkington, T. R. DeGrado, and W. H. Sampson, "Small spheres for lesion detection phantoms," in *2001 IEEE Nuclear Science Symposium Conference Record* (IEEE, San Diego, CA, 2001), Vol. 4, pp. 2234–2237.
[3]P. J. Markiewicz, G. I. Angelis, F. Kotasidis, M. Green, W. R. Lionheart, A. J. Reader, and J. C. Matthews, "A custom-built PET phantom design for quantitative imaging of printed distributions," Phys. Med. Biol. **56**, N247–N261 (2011).
[4]M. Miller and G. D. Hutchins, "Development of anatomically realistic PET and PET/CT phantoms with rapid prototyping technology," in *2007 IEEE Nuclear Science Symposium Conference Record* (IEEE, Honolulu, HI, 2007), pp. M26–M28.
[5]D. C. Hunt, H. Easton, and C. B. Caldwell, "Design and construction of a quality control phantom for SPECT and PET imaging," Med. Phys. **36**(12), 5404–5411 (2009).
[6]J. I. Gear, C. Long, D. Rushforth, S. J. Chittenden, C. Cummings, and G. D. Flux, "Development of patient-specific molecular imaging phantoms using a 3D printer," Med. Phys. **41**, 082502 (3pp.) (2014).
[7]3d Systems, "ProJet 3500 SD and HD professional 3D printers," Web. 5 June 2015, http://www.3dsystems.com/sites/www.3dsystems.com/files/projet_3500_plastic_usen.pdf.
[8]P. Olcott, E. Kim, K. Hong, B. J. Lee, A. M. Grant, C. M. Chang, G. Glover, and C. S. Levin, "Prototype positron emission tomography insert with electro-optical signal transmission for simultaneous operation with MRI," Phys. Med. Biol. **60**(9), 3459–3478 (2015).
[9]J. Cui, G. Pratx, B. Meng, and C. S. Levin, "Distributed MLEM: An iterative tomographic image reconstruction algorithm for distributed memory architectures," IEEE Trans. Med. Imaging **32**(5), 957–967 (2013).